# Overview and Highlights of WOLEDs and Organic Solar Cells: From Research to Applications

**Maggie Mei-Yee Chan, Chi-Hang Tao, and Vivian Wing-Wah Yam**

## Contents

**Abstract** Solid-state organic devices are at the vanguard of new generation of electronic components owing to their promise to be easily manufactured onto flexible substrates that potentially reduce the mass production cost for large modules. With the great efforts on improving the power efficiency that meets the realistic requirements for commercial applications, white organic light-emitting devices (WOLEDs) and organic solar cells have attracted much attention over the past two decades and are targeted as the effective ways for reducing the energy consumption and developing renewable energy in the world. Because of their great potentials to generate tremendous savings in both cost and energy usage, WOLEDs are considered as new generations of solid-state lighting sources to replace the incandescent bulbs, while organic solar cells are the most promising candidates to complement the inorganic silicon solar cells for electricity generation. Here, we

---

M.M.-Y. Chan, C.-H. Tao, and V.W.-W. Yam (✉)
Department of Chemistry, The University of Hong Kong, Pokfulam Road, Hong Kong, China
e-mail: wwyam@hku.hk

V.W.W. Yam (ed.), *WOLEDs and Organic Photovoltaics*, Green Energy and Technology,
DOI 10.1007/978-3-642-14935-1_1,

will provide a survey on the recent developments of WOLEDs and organic solar cells and their current status in these fields. Resistances and hampers to the widespread acceptances of these two areas of developments are also discussed.

## 1 Introduction

Energy is essential to our life, and the use of energy is increasing with human advancement and industrial development. According to the recent report on the international energy outlook (IEO) [1], the energy information administration (EIA) predicts that the world demand for energy will increase by 44% from 2006 to 2030, in which the total world energy consumption will rise from 472 quadrillion British thermal units (QBtu), or Quads, in 2006 to 678 Quads in 2030 at an average annual rate of 1.8%. Strong gross domestic product (GDP) growth and industrialization in emerging markets, especially in China and India, will drive the fast-paced growth in energy demand. Particularly, total energy demand in these emerging markets increases by 73%, compared with an increase of 15% in the industrialized nations such as the United States and Europe.

Currently, nearly all energy production comes from the burning of fossil fuels, including oil, coal, and natural gas. With the current trend of energy use, approximately 17,000 million tons of oil or 24,400 million tons of coal, will be consumed to meet the tremendous demand for energy in 2030. These increasing energy demands continue to push oil price higher and higher. The average world oil prices increased each year between 2003 and 2008. Spot prices reached US$147 per barrel in mid-July 2008. In the IEO 2009, EIA predicts that the price of oil will rise from US$61 per barrel in 2009 to US$130 per barrel in 2030 [1]. The worldwide increase in energy demand has put an ever-increasing pressure on identifying and implementing ways to save energy and to take measures to promote it. Indeed, many nations have committed on their new energy policies to improve energy efficiency. For example, Australia became the first country to announce an outright ban on incandescent bulbs starting in 2010. On 17 December 2007, President George W. Bush signed into law a landmark energy bill to begin phasing out traditional incandescent bulbs starting in 2012, to be completed in 2014. In particular, lighting accounts for a significant part of electricity consumption in the world. For instance, about 40% of all consumed energy (40.25 of 100 Quads) was used in commercial and residential buildings in the United States in 2007, and 14% of that (5.74 Quads) was used just for lighting [2]. In fact, consumers and businesses spend approximately US$58 billion a year to light their homes, offices, streets, and factories. It is clear that increasing the efficiency of lighting by a small amount has the potential to generate tremendous savings in both cost and energy use. In fact, the US Department of Energy is now anticipating that solid-state lighting in the form of white inorganic light-emitting diodes (WLEDs) and white organic light-emitting devices (WOLEDs) will decrease national energy consumption by 29% by 2025, cutting US$125 billion off the national energy bill and deferring the construction of forty 1,000 MW power plants for electricity generation [3].

Meanwhile, many nations dedicate to develop renewable energy for promoting their energy supply. On 29 April 2009, US President Barack Obama pledged to achieve its renewable objectives to make up 20% of power to be generated by wind, and for solar power to be market competitive by 2015. Renewable energy is the kind of energy generated from natural resources, including sunlight, wind, rain, tides, and geothermal heat, which can be replenished rapidly and constantly. Harvesting solar energy is an attractive option among the alternatives and presents the greatest opportunity for meeting the energy demand in a clean and renewable way. According to the US Department of Energy, the energy from sunlight strikes the earth in one hour (approximately 120,000 TW) is more than the energy we consumed in a year (~15 TW) [4]. In this chapter, we survey the recent developments on WOLEDs and organic solar cells and the current status and challenges in these fields.

## 2 White Organic Light-Emitting Devices

Lighting is an essential commodity of our life since the invention of incandescent light bulb by Thomas Edison in 1880. According to the Navigant 2002 annual report [5], the incandescent lamps were responsible for the 86% of the total lighting electricity consumption in the United States residential buildings, while fluorescent lamps shared only 14%. However, approximately 90% of the power consumed by an incandescent light bulb is lost as heat, rather than as visible light. With the efforts of researchers and industries, various white lighting sources, including compact fluorescent lamp (CFL), fluorescent tube, WLED, and WOLED, have been introduced. Especially, due to the significant energy saving as well as the increased lifetimes over standard incandescent lighting, WLEDs and WOLEDs have been considered as the new generation of lighting sources to replace the incandescent lamps in the near future.

### *2.1 Advantages of WOLEDs*

Compared with the inorganic counterpart, WOLEDs have several advantages as a replacement of conventional lighting. In fact, WOLEDs were targeted toward display applications for use primarily as liquid-crystal display backlights. As their power efficiencies have surpassed those of incandescent lamps due to improvements in device architectures, and synthesis of novel materials, interest in the application of WOLED technology for solid-state lighting has been steadily increasing. A comparison of various lighting sources is provided in Table 1.

**Table 1** Power efficiency ($\eta_P$), power consumption at brightness of 800 lm, chromaticity coordinates, CCT, CRI, and lifetime of various lighting sources available on the market

| Type | $\eta_P$ (lm W$^{-1}$) | Power consumption (W) | CCT (K) | CRI | Lifetime (h) |
|---|---|---|---|---|---|
| Incandescent lamp | 15 | 60 | 2,854 | 100 | 1,500 |
| CFL (warm) | 60 | 15 | 2,940 | 82 | 10,000 |
| LED | 90 | 8 | 3,000 | 80 | 60,000 |
| WOLED | 102[a] | – | 3,900 | 70 | – |

[a] Maximum power efficiency of lighting sources reported in the literature

WOLEDs offer distinct properties to replace classical light bulbs or even fluorescent tubes. In particular, WOLEDs can be used as an ultrathin area light source, emitting diffuse light from a potentially large active area. They do not need light distribution elements, and its thickness could reach less than 1 mm that could allow the lighting to be placed directly on ceilings as a planar sheet of light. WOLEDs are also fully dimmable and can be switched on and off without any time delay. It is worth noting that being an area light source, the heat generation inside the device is not focused on a small volume as it is the case in LEDs; particularly, during standard operation, the self-heating of an OLED is limited to only a few degrees. WOLEDs are also possible to have transparent panels, which could be used as lighting elements in windows, screens, or room dividers. Most importantly, WOLEDs can be fabricated onto flexible substrates to provide new architectural design opportunities that cannot be realized with any other technology.

## 2.2 *Efficiency Characterization of WOLEDs*

WOLEDs show promise as substitutes of incandescent or fluorescent bulbs in future ambient lighting, due to favorable properties such as large area emission and potential fabrication on flexible substrates. Many smart materials and novel device configurations have been used to improve the device performance; particularly, recent demonstrations have shown continually improved WOLEDs that are now surpassing incandescent lamps in terms of efficiency and lifetime [6–8]. To turn a WOLED into a power-efficient light source, four key parameters must be addressed for evaluating the performance of WOLEDs (1) luminous power efficiency, (2) the Commission Internationale de L'Éclairage (CIE) chromaticity coordinates, (3) the correlated color temperature (CCT), and (4) the color rendering index (CRI).

*Luminous power efficiency*, $\eta_P$, or simply called "power efficiency", in lumen per Watt [lm W$^{-1}$] is the ratio of luminous power emitted in the forward direction, $L_P$ [lm], to the total electrical power required to drive the OLED at a particular voltage, $V$, and current, $I_{OLED}$, viz.: $\eta_P = L_P/I_{OLED}\,V$ [9]. It is very useful in interpreting the power dissipated by a device when used in a display or lighting source. Lumen is a measure of the amount of light given off by a light source. A typical 60 W incandescent bulb gives off 840 lm, and a 100 W incandescent bulb gives off

1,750 lm. As a lighting source, the $\eta_P$ of WOLEDs should be larger than that of fluorescent tubes (~60 lm $W^{-1}$), which is the current benchmark for novel light sources.

*CIE chromaticity coordinates* is the predominant, international standard for color specification and measurement. Generally, the CIE color system established in 1931 is based on the eye response of standard observers on three specific wavelengths of light in the red–green–blue (RGB) regions (700.0 nm, 546.1 nm, and 435.8 nm, respectively) [10]. Three $XYZ$ tristimulus values are then derived from the relative amounts of these characteristic wavelengths present in a color. The tristimulus values $XYZ$ are useful for defining a color, but the results are not easily visualized. Instead, a color space ($Y, x, y$) is commonly used. $Y$ is the intensity of light (that is identical to the tristimulus value $Y$), and $x$, $y$ are chromaticity coordinates calculated from the tristimulus values $XYZ$ by

$$x = \frac{X}{X+Y+Z}, \; y = \frac{Y}{X+Y+Z} \; . \qquad (1)$$

Figure 1 shows a CIE 1931 chromaticity chart for this color space. All perceived colors could be defined in this horseshoe shaped region, at which the achromatic point (0.33, 0.33) represents the "pure" white light.

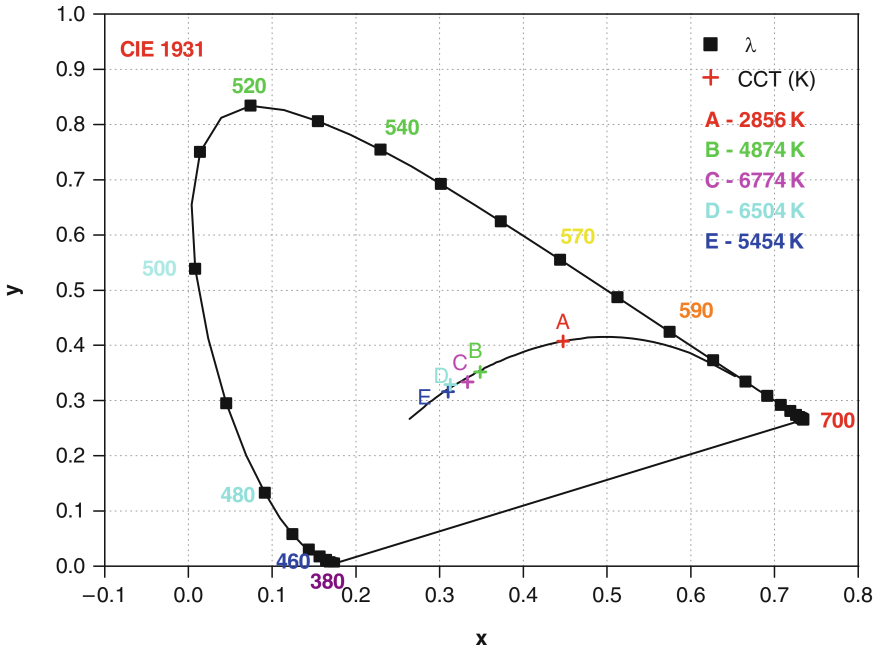

**Fig. 1** CIE 1931 chromaticity chart with CRI of the common standard illuminants

*CCT* is the temperature of a blackbody radiator that has a color that most closely matches the emission from a nonblackbody radiator [11]. It is a measure used to describe the "whiteness" of a light source. The higher is the color temperature, the cooler the white light will be. Incandescent bulbs and CFLs are usually around 2,800 K and fall in the 2,700–3,000 K range, respectively, which are "warm" light, while a cool white light LED has a CCT of 6,500 K.

*CRI* of a white light source is a measure of the color shift that an object undergoes when illuminated by the light source as compared to the color of the same object when illuminated by a reference source of comparable color temperature [12, 13]. It is an international system used to rate a lamp's ability to show an object's color. The higher the CRI, based on a scale of 0–100, the truer colors will appear. Acceptable illumination sources require a CRI of higher than 80, provided that the natural sunlight has a CRI of 100.

It is worth noting that the color of two white light sources may appear identical, when viewed directly, and will therefore have the same chromaticity; however, the color of the reflected light from an object illuminated by these two sources may be significantly different, and thus the light sources will have a different CRI. For high-quality white light illumination, sources with CIE coordinates similar to that of a blackbody radiator with a CCT between 2,500 and 6,500 K, and a CRI above 80 are required. Table 2 illustrates the color quality of the common CIE standard illuminants.

## 2.3 WOLED Architectures

White light emission is achieved by mixing the complementary (e.g., blue and yellow or orange) colors or the three primary colors (red, green, and blue). With the continuous efforts on research activities, the $\eta_P$ of WOLEDs have surpassed those of incandescent sources and are now approaching that of fluorescent tubes. Several strategies have been proposed to generate white light, including (1) doping fluorescent or phosphorescent materials into one or more light-emitting layers (EMLs) [14–23], (2) synthesis of novel metal complexes incorporating different color-emitting moieties [24, 25], (3) use of excimer or exciplex systems [26–31], (4) tandem structure [32–36], and (5) down-conversion architectures [37, 38]. Among these approaches, the incorporation of phosphorescent emitters is the most effective way for achieving WOLEDs. The use of phosphors can harvest both the singlet and

**Table 2** CCT and CIE 1931 coordinates of the common CIE standard illuminants [12]

| Illuminant | CCT (K) | CIE 1931 |
|---|---|---|
| A | 2,856 | 0.4476, 0.4075 |
| B | 4,874 | 0.3485, 0.3517 |
| C | 6,774 | 0.3101, 0.3163 |
| D65 | 6,504 | 0.3127, 0.3291 |
| E | 5,400 | 0.3333, 0.3333 |

triplet excitons (generated at a ratio of 1:3 owing to their statistical spin population) generated by electrical injection, corresponding to a fourfold increase in internal quantum efficiency, that is the ratio of the total number of photons generated within the device to the number of electrons injected, compared to that achievable in singlet-harvesting fluorescent WOLEDs. Indeed, a high $\eta_P$ of 102 lm $W^{-1}$ has been recently realized in all phosphor-doped WOLEDs [6]. Particularly, phosphorescent emitters are doped into conductive hosts in either single emitting layer or multiple EMLs, where two or more emission centers are physically separated from each other. In general, there are three device architectures of phosphorescent WOLEDs that are often exploited. They are described as follows.

### 2.3.1 WOLEDs with Single Emitting Layer

Incorporation of two or three phosphorescent materials into a single host to generate white light is the simplest method for achieving WOLEDs. The key feature of this approach is the employment of one EML that comprises of a large bandgap host doped with two or more emissive phosphorescent dopants to generate white light [14–18]. A desired electroluminescence (EL) performance can be achieved just by optimizing the composition of this EML and the adjacent functional layers. This method allows the fabrication processes to be simplified as well as reduces structural heterogeneities, and produces rather stable EL spectra, suggesting its great potential for mass production and commercial realization in the future. In 2004, D'Andrade et al. [14] demonstrated the performance of WOLED that employed an EML containing three metal organic phosphors: 2 wt% iridium(III) bis(2-phenylquinolyl-*N*,$C^{2'}$)acetylacetonate [PQIr] providing red emission, 0.5 wt% *fac*-tris(2-phenylpyridine)iridium [$Ir(ppy)_3$] for green emission, and 20 wt% iridium(III) bis(4′,6′-difluorophenylpyridinato)tetrakis(1-pyrazolyl)borate [FIr6] for blue emission, all simultaneously codoped into a wide energy gap *p*-bis(triphenylsilyl)benzene (UGH2) host. Such triple-doped WOLED exhibited a maximum $\eta_P$ of 42 lm $W^{-1}$ [corresponding to an external quantum efficiency (EQE) of 12%], and CIE coordinates of (0.43, 0.45) with CRI of 80. Eom et al. [16] further improved the EL efficiency of these WOLEDs by utilizing dual triple-doped emissive layers, in which three phosphorescent dopants [PQIr, $Ir(ppy)_3$, and FIr6] were codoped into two adjacent wide bandgap hosts, namely, *N*,*N*′-dicarbazolyl-3,5-benzene (mCP) and UGH2. Figures 2 and 3 show the chemical structures of the phosphors and the host materials employed for WOLEDs, respectively. This double EML structure broadened the exciton recombination zones, resulting in a significant improvement in $\eta_P$ of 26 lm $W^{-1}$, at a luminance of 1,000 cd $m^{-2}$, doubling that of triple-doped WOLEDs reported by D'Andrade et al. ($\eta_P = 11$ lm $W^{-1}$) [14]. With balanced emission from the three emitting layers, white light emission with CRI of 79 and CIE coordinates of (0.37, 0.40) could be achieved.

WOLEDs can also be prepared by the combination of two complementary colors (blue and yellow or orange). Wang et al. [17] recently reported a highly efficient WOLED by incorporating two phosphorescent dyes, namely, iridium(III)

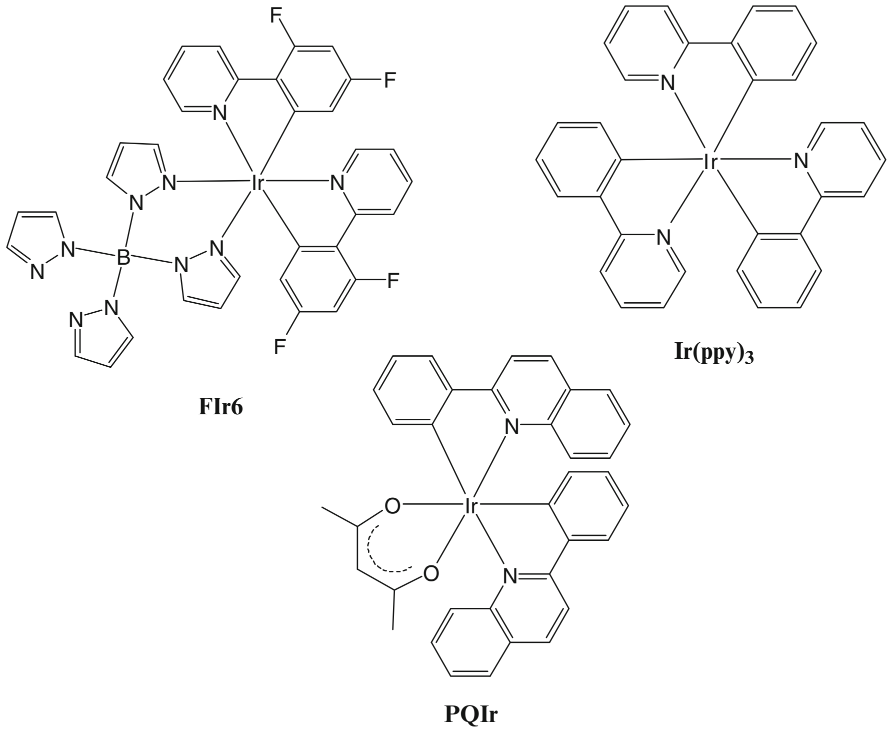

**Fig. 2** Chemical structures of phosphors used for WOLEDs

[bis(4,6-difluorophenyl)-pyridinato-*N*,$C^2$]picolinate [FIrpic] doped into mCP for blue emission and bis(2-(9,9-diethyl-9*H*-fluoren-2-yl)-1-phenyl-1*H*-benzoimidazol-*N*,$C^3$)iridium (acetylacetonate) [$(fbi)_2Ir(acac)$] doped into 4,4′,4″-tri(*N*-carbazolyl)triphenylamine (TCTA) for orange emission, into a single-energy well-like emissive layer. Figure 4 depicts the chemical structures of [$(fbi)_2Ir(acac)$] and TCTA. Such device achieved a peak forward-viewing $\eta_P$ of 42.5 lm $W^{-1}$, corresponding to EQE of 19.3%, a current efficiency (or sometimes called “luminous efficiency”) of 52.8 cd $A^{-1}$, and excellent color stability with CIE coordinates of (0.30, 0.37) at luminance of 1,000 cd $m^{-2}$. Particularly, the key feature for extremely high $\eta_P$ and EQE is related to the careful manipulation of two exciton-formation modes, namely host–guest energy transfer for the blue dopant and direct exciton formation for the orange dopant within an energetic, well-like, single emissive region. This unique strategy created two parallel pathways to channel the overall excitons to both dopants within the EML, leading to an improved charge balance and further reduction of the unfavorable energy losses. Hence, an extremely high efficiency WOLED with nearly 100% internal quantum efficiency could be realized.

However, in most conventional single-EML WOLEDs, it is quite difficult to obtain a common host material with a wide bandgap and large triplet energy

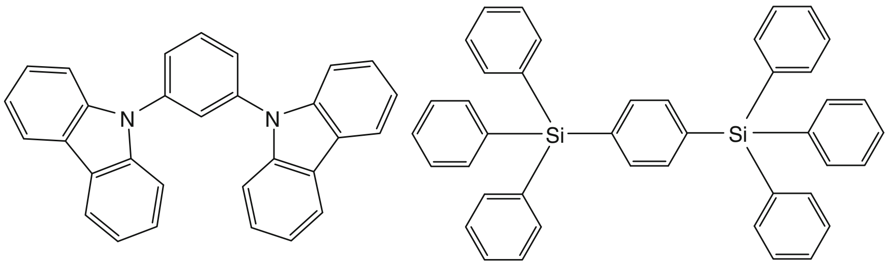

**mCP** **UGH2**

**Fig. 3** Chemical structures of host materials used for WOLEDs

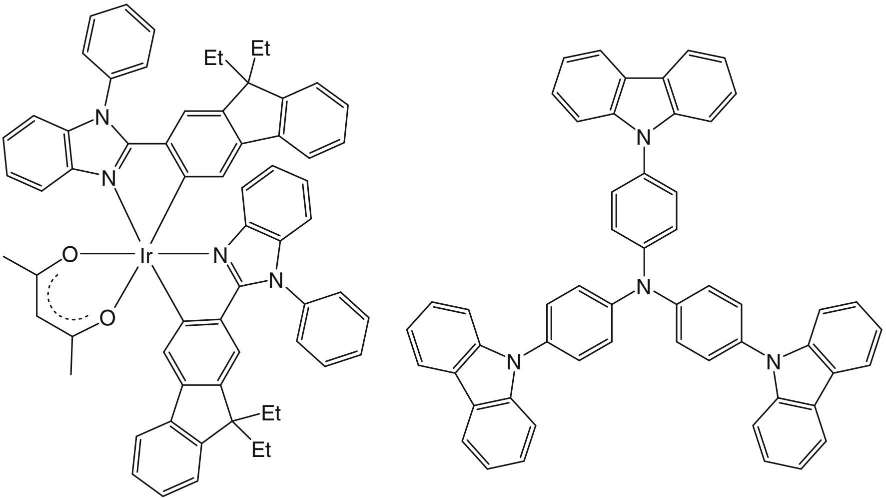

**(fbi)$_2$Ir(acac)** **TCTA**

**Fig. 4** Chemical structures of [(fbi)$_2$Ir(acac)] and TCTA

($>$2.8 eV) to efficiently transfer energy from the host to all the three dopants [15, 18]. In addition, sequential energy transfer initially from the short-wavelength dopant always dominates the main emission mechanism. Indeed, the majority of excitons are generated by Dexter energy transfer from the host or trapping on the blue-emitting molecules, and then subsequently transferred to the green and red dopants [19, 20]. Hence, the EQE of the entire device is limited by the less-efficient blue species. Furthermore, host materials that have wider bandgaps will act as energy barriers for the transport of carriers from nearby hole or electron-transporting layer to EMLs, which consequently decrease the probability of carrier recombination. Particularly, WOLEDs with single EML usually have higher operating voltage [17].

### 2.3.2 Phosphorescent WOLEDs

To date, the most impressive characteristics of WOLEDs reported have been achieved in all-phosphor-doped devices, in which three phosphorescent dopants (red, green, and blue) are intentionally doped into three separate EMLs [20, 21]. The key feature of this WOLED is the positioning of blue phosphor within the emission layer and its combination with a carefully chosen host material: energetically, (1) the triplet energy of the blue emitter material is in resonance with its host, so that the blue phosphorescence is not accompanied by internal triplet energy relaxation before emission and (2) triplet energies of all materials, that is, the host materials and the adjacent hole- and electron-transporting materials, should have higher triplet energies than that of the phosphorescent emitters. This can essentially define the exciton distribution within the multilayer emission layer. With good knowledge on device engineering, multiple EMLs effectively broaden the exciton recombination zone and reduce the pile-up of excitons at the EML, thereby enhancing EL efficiency and reducing the efficiency roll-off. In particular, triplet–triplet annihilation is the main mechanism for unusual strong efficiency roll-off at high current densities and luminance [22]. It is reported that the degree of triplet–triplet annihilation is proportional to the square of the triplet exciton density, and a narrow emission zone has been found to have a negative effect on triplet–triplet annihilation due to its high triplet exciton density [22]. Maximizing the recombination zone thus effectively suppresses the triplet–triplet annihilation and reduces the efficiency roll-off.

Sun and Forrest [21] had successfully demonstrated a highly efficient WOLED by employing three adjacent phosphorescent EMLs. The phosphorescent dopants, namely, [PQIr] for red, [Ir(ppy)$_3$] for green, and [FIr6] for blue emissions, were each doped in separate hosts that form a stepped progression of highest occupied and lowest unoccupied molecular orbitals. This structure effectively broadened exciton generation region, as well as allowed for separate optimization of the three dopant–host material combinations across the three hosts. Such 3-EML WOLED exhibited high peak forward-viewing $\eta_P$ and EQE of 32 lm W$^{-1}$ and 16%, respectively, and good CIE coordinates of (0.37, 0.41) with CRI of 81. Very recently, WOLED with fluorescent tube efficiency had been realized, as reported by Reineke et al. [6]. This three-EML device combined a novel concept for energy-efficient photon generation with an improved out-coupling, in which blue-emitting layer was surrounded by red and green sublayers of the emission layer to harvest unused excitons. By combining a carefully chosen emitter layer with high refractive index substrates, and using a periodic out-coupling structure, an extremely high $\eta_P$ of 90 lm W$^{-1}$ at luminance of 1,000 cd m$^{-2}$ could be achieved. This efficiency has the potential to be raised to 124 lm W$^{-1}$ (corresponding to EQE of 46%) if the light out-coupling can be further improved.

As the $\eta_P$ of WOLEDs employing multiple EMLs approaches fluorescent tube efficiency, it requires a careful control of the location of exciton recombination and the energy transfer/exciton diffusion between or within layers, via the changing of layer thickness, doping concentration, and charge blocking layers, in order to obtain a balanced white light emission. In addition, as one of the three primary colors, the maximum EQE of blue OLEDs are comparatively lower than those reported for green and red OLEDs [19]. While suitable molecules have been found for the green and red, stable and efficient blue phosphorescent emitters are still a challenge, and this inevitably limits the efficiency of WOLEDs with multiple EMLs.

### 2.3.3 Hybrid WOLEDs

For power-efficient phosphorescent WOLEDs, an additional challenge is that high energy phosphors demand host materials with even higher triplet energies to confine the exciton to the emitter. This problem can be eliminated by introducing a novel device concept that exploits a blue fluorescent molecule with high triplet energy in exchange for a phosphorescent dopant, in combination with green and red phosphor dopants [8, 19, 20, 22], to yield high $\eta_P$ and stable color balance, while maintaining the potential for unity internal quantum efficiency. In short, this structure takes advantage to harness all electrically generated high-energy singlet excitons for blue emission, and phosphorescent dopants to harvest the remainder of lower energy triplet excitons for green and red emission.

In 2006, Sun et al. [19] illustrated the effectiveness of this WOLED architecture by doping the middle region of the EML with both the green [Ir(ppy)$_3$] and red [PQIr] phosphorescent dopants sandwiched between two blue fluorescent-doped EMLs. The key feature of this WOLED structure was that the phosphor-doped region was separated from the exciton-formation zones by spacers of undoped host material. The triplet excitons then diffused efficiently to the central region, where they transferred to the lower energy green or red phosphor dopants, again by a nearly resonant process to the green dopant triplet manifold, and with some energy lost to the red triplet. Diffusion of singlet excitons to the phosphorescent dopants was negligible due to their intrinsically short diffusion lengths. The optimized device exhibited a high $\eta_P$ and total EQE of 37.6 lm W$^{-1}$ and 18.7%, respectively. In addition, the CIE coordinates had a negligible shift from (0.40, 0.41) at low current densities to (0.38, 0.40) at 100 mA cm$^{-2}$. It is also worth noting that the optimized WOLED had a less-pronounced efficiency roll-off at high current densities, as compared to previous all-phosphor, high-efficient WOLEDs.

Schwartz et al. [22] modified this WOLED architecture by employing a fluorescent blue emitter, *N*,*N*′-di-1-napthalenyl-*N*,*N*′-diphenyl-[1,1′:4′,1″:4″,1‴-quaterphenyl]-4,4‴-diamine (4P-NPD) (as shown in Fig. 5), with very high triplet energy of 2.3 eV and high photoluminescence (PL) quantum yield of 92%, rendering it possible to harvest its triplet excitons by letting them diffuse to an orange phosphorescent iridium complex. Such WOLED exhibited a total $\eta_P$ of 57.6 lm W$^{-1}$ at a brightness of 100 cd m$^{-2}$ (corresponding to an EQE of 20.3%). Later, they demonstrated an improved device structure by directly doping the orange phosphorescent material into the blue fluorescent EML with low concentration (0.2 wt%) to decouple the strong efficiency roll-off [8]. The modified WOLED

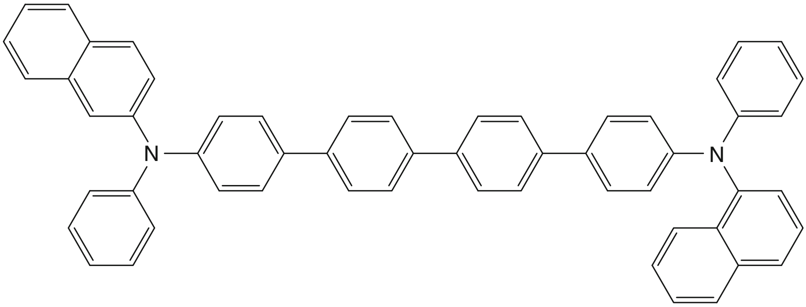

**4P-NPD**

**Fig. 5** Chemical structure of 4P-NPD

yielded a total $\eta_P$ of 49.3 lm $W^{-1}$ and total EQE of 24.1%, measured in an integrating sphere, and CIE coordinates of (0.49, 0.41) with CRI of 82.

A key prerequisite for this hybrid WOLED concept is choosing a suitable blue fluorescent-emitting material that should have a high triplet energy as well as high PL quantum yield. However, up until now, there is only limited choice on the blue fluorescent emitter. Particularly, triplet excitons, which are either directly generated on or transferred by Dexter transfer to the blue emitter, are being lost [22]. This is a result of the excitons' inability to leave the blue emitter because of its low-lying triplet state. Hence, rather low efficiencies can only be achieved for most of the hybrid WOLEDs at an illumination relevant brightness, say, 1,000 cd $m^{-2}$ [8].

## 2.4 Challenges of WOLEDs

As the development of novel organic materials and smart device design further improves the performance of WOLEDs, the major challenge for the commercialization of WOLED as solid-state lighting is the operational lifetime. Typically, fluorescence bulbs have lifetimes of ~10,000 h. However, the operational lifetimes of the reported blue phosphorescence devices are significantly short; for example, the luminance of the FIrpic-based blue phosphorescent device drops to 50% of its initial value within 1–2 h [6]. To compete as a light source in the general illumination, market will require a product life of tens of thousands of hours. End of life will be determined when the original luminance intensity of the device decreases to 70% of the original value, versus 50% as often referenced for display applications. As the product ages, the color is not expected to change. In other words, the relative intensity of the respective color sources should remain constant over the life of the product.

Another major challenge facing this WOLED technology for general illumination purposes is reducing the cost per lumen. As lighting is not a new market, WOLEDs must be cheaper than the current technology in order to be adopted. The decorative lighting market has the least stringent requirements and requires a brightness of 50–500 cd $m^{-2}$ at an efficiency of >10 lm $W^{-1}$ for an operational lifetime of at least 10,000 h. The market for general illumination requires much larger panels at high brightness (5,000 cd $m^{-2}$) and very high efficiencies of >50 lm $W^{-1}$. If the cost of an 800 lm WOLED comes down even to US$3.00 per megalumen-hour, it makes economic sense to be widely adopted.

## *2.5 Lighting for the Future*

Through continuing efforts on improving luminance efficiency, color gamut, and device reliability, WOLEDs have a great potential to replace or complement other lighting technologies and becomes the light source of choice for the future. According to the recent NanoMarkets report "OLED Lighting Markets" [39], there are great commercial opportunities for OLED lighting used for backlighting, general illumination, specialty/architectural lighting, vehicular lighting, signage, and niche applications. Meanwhile, the US Department of Energy expects OLED lighting to reach a high $\eta_P$ of 150 lm $W^{-1}$ in 2012 rather than 2014 as previously forecasted [40]. NanoMarkets believe that these and other improvements in OLEDs will drive the general illumination market to US$2.3 billion in revenues by 2015. In particular, the OLED backlighting market will reach US$1.1 billion by 2015, while OLED architectural and specialist industrial lighting will reach US$1.9 billion.

With the advent of commercial interest in WOLED, many anticipative applications have been demonstrated. For example, on the Plastic Electronics Asia 2009, Fraunhofer Institute for Photonic Microsystems IPMS demonstrated a steering wheel with an integrated OLED signage device for automotive applications (Fig. 6) [41]. This OLED device was made within the German joint development

**Fig. 6** Steering wheel with an integrated OLED signage device demonstrated by the Optrex Europe GmbH, Fraunhofer Institute for Photonic Microsystems IPMS, and G. Pollmann GmbH under the German joint development project CARO (Car OLED). Reproduced with permission from [41]. Copyright 2009, Optrex Europe GmbH

project CARO (Car OLED) among Optrex Europe GmbH, Fraunhofer Institute for Photonic Microsystems (Fraunhofer IPMS), and the styling-studio G. Pollmann GmbH. Meanwhile, OSRAM Opto Semiconductors GmbH had developed a transparent WOLED with outstanding performance (Fig. 7) [42]. The WOLED prototype lighted up an area of nearly 90 cm$^2$, with $\eta_P$ of more than 20 lm W$^{-1}$ at a brightness of 1,000 cd m$^{-2}$ and CIE coordinates of (0.396, 0.404). This WOLED was transparent whether it is powered on or off, and its transparency was currently rated at 55%. This opens up possible applications such as partitions that are almost invisible by day and then provides a pleasant diffused light at night. In March 2008, GE Global Research and GE Consumer and Industrial successfully demonstrated “the world’s first roll-to-roll manufactured OLED lighting devices,” as shown in Fig. 8 [43].

In April 2008, OSRAM Opto Semiconductors GmbH presented the first WOLED product “Early Future” at the Light & Building Fair in Frankfurt, Germany [42]. This WOLED table lamp is designed by a renowned lighting designer Ingo Maurer and is being produced as a limited edition. It works with ten WOLED tiles, each measures at 132 × 33 mm, at luminance of 1,000 cd m$^{-2}$ and $\eta_P$ of 20 lm W$^{-1}$, as shown in Fig. 9. Mercedes Benz recently announced a new 2010 Mercedes Benz E-class equipped with an elegant control panel that uses a WOLED as the display (Fig. 10) [44]. These revolutionary application marks the emergence of a new technology of lighting.

## 3 Organic Solar Cells

As mentioned in Sect. 1, the global demand for energy is continually expanding, that the total world energy use will increase at an average annual rate of 1.8% and reaches 678 Quads (~18.49 TW) in 2030. Currently, nearly all energy production comes from the burning of fossil fuels, such as oil, coal, and natural gas. Through the incremental improvement on the renewable energy technologies, including hydroelectric, geothermal, tidal, wind, and biomass, harnessing solar energy is an attractive option among the different carbon-free alternatives. Table 3 summarizes the energy supply from the renewable energy technologies. Approximately 89,000 TW of solar energy strikes the earth’s surface each year, and the capture of a fraction of solar energy can supply all of our energy needs in 1 year, that is, the world energy demand in 2008 is equal to 15 TW. As solar energy offers great potential for the supply of all our energy demand, solar cell technology has experienced rapid growth in recent years as the costs have improved. According to the recent research report “World Solar Cell Market: Key Research Findings 2009” issued by Yano Research Institute, the global solar cell production had been increased by 69% from 3.8 GW in 2007 to 6.5 GW in 2008 [45]. Meanwhile, many companies are planning to enter the solar cell business by building their production line. For instance, in 2008, LG Electronics, a global leader and technology innovator in consumer electronics, decided to convert its plasma panel-manufacturing

**Fig. 7** Transparent WOLED prototype from OSRAM Opto Semiconductors GmbH. Reproduced with permission from [42]. Copyright 2009, OSRAM Opto Semiconductors GmbH

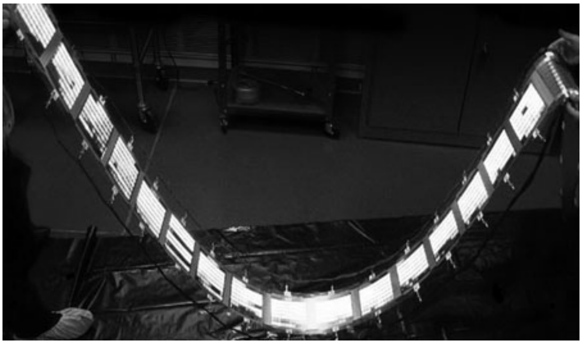

**Fig. 8** The world's first roll-to-roll manufactured OLED lighting devices from GE Global Research and GE Consumer & Industrial. Reproduced with permission from [43]. Copyright 2009, General Electric Company

**Fig. 9** OSRAM Early Future OLED lamp designed by a renowned designer Ingo Maurer. Reproduced with permission from [42]. Copyright 2009, OSRAM Opto Semiconductors GmbH

**Fig. 10** The 2010 Mercedes Benz E-Class control panel. Reproduced with permission from [44]. Copyright 2009, Dailmer AG

**Table 3** Energy supply from the renewable energy resources in 1 year

| Resources | Energy supply (TW) |
|---|---|
| Hydropower | 0.5 |
| Geothermal | 12 |
| Tidal | 2 |
| Wind | 5 |
| Solar | 89,000 |
| Biomass | 1.7 |

line in Gumi, Korea, into solar cell production lines and planned to manufacture crystalline silicon solar cells and modules with a capacity of 120 MW each [46].

Solar cells generate power by converting photons from the sun into electricity through a mechanism called "the photovoltaic effect." The term "photo" means light and "voltaic" means electricity. A solar cell is primarily constructed of inorganic semiconductor that generates electricity when sunlight falls on it. Nowadays, most of the solar cells are silicon based, in which their power conversion efficiencies (i.e., the efficiency to convert incident solar power to useful electric power) can achieve up to 23.2%, reported by a research team from Eindhoven University of Technology together with the Fraunhofer Institute in Germany [47]. The US Department of Energy's National Renewable Energy Laboratory (NREL) has recently developed a triple-junction solar cell that can convert 40.8% of sunlight into electricity under concentrated light of 326 suns [48]. Meanwhile, the University of Delaware has broken the world record for solar cell to 42.8% by using an optical concentrator to split light into components, i.e., high, medium, and low energy light, and direct it to several different materials which can then extract electrons out of its photons [49]. With the great effort on improving the efficiency of solar cells, their costs have been rapidly reduced. In 1956, silicon cells cost approximately US$300 per Watt of electricity produced. Today, the solar cells have dropped in cost to approximately US$1.3 per Watt [50]. However, this cost is still too high to be competitive against relatively plentiful and cheap fossil fuels. In order for large-scale adaptation of this technology, the cost of solar cells needs to be dropped by at least a factor of 10 in order to be on par with current means of electricity generation. There is a prevailing need for the development of new materials and concepts for photovoltaic energy conversion that could potentially reduce the manufacturing cost of solar cells.

### *3.1 Basic Working Principle of Organic Photovoltaic Devices*

The development of dye-sensitized solar cell and organic photovoltaic (OPV) devices, so-called "third and fourth generation" solar cells, has been envisaged as a possible route. In this chapter, the field of OPV devices will be briefly introduced. OPV devices provide many foreseeable advantages, including simple fabrication process, light weight, flexibility, and solution processability for large area production. These, together with the virtually infinite variety of molecules to choose from and design that show very strong optical absorption with tunable absorption and electrical properties, would make them very attractive. OPV devices generally consist of two photoactive organic materials (so-called "donor–acceptor" system) sandwiched between two conducting electrodes. Under light illumination, excitons are generated in the photoactive layers and some would dissociate into electrons and holes at the donor–acceptor heterointerfaces. Alternatively, some excitons may diffuse to the electrode and decay nonradiatively via quenching and releasing energy in the form of a phonon as heat. These charge carriers are subsequently collected at the respective electrodes, contributing to the photocurrent [51–54]. It is worth noting that the process of photocurrent generation by an OPV device is analogous to the basic working principle of OLED. Particularly, OLED is a device that converts electrical energy into light, while OPV is a device that converts the energy of sunlight directly into electricity. Figure 11 illustrates the schematic diagram of the basic working principle of an OPV device. The process of converting light into electric current in an organic OPV device is accomplished by four consecutive steps (1) Light absorption leading to the formation of an excited electron–hole pair (exciton); (2) exciton diffusion to the donor–acceptor heterointerfaces, where (3) the exciton dissociation occurs into a free electron and hole by charge transfer; (4) finally the charge carriers are collected at the anode (holes) and cathode (electrons), providing current to a load in the external circuit. In short, the external quantum efficiency ($\eta_{\mathrm{EQE}}$) of an OPV device is defined as the ratio of the number of electron–hole pairs collected at the electrodes to the number of incident photons [52, 53], viz.,

$$\eta_{\mathrm{EQE}} = \eta_{\mathrm{A}}\eta_{\mathrm{ED}}\eta_{\mathrm{CT}}\eta_{\mathrm{CC}}, \tag{2}$$

where $\eta_{\mathrm{A}}$, $\eta_{\mathrm{ED}}$, $\eta_{\mathrm{CT}}$, and $\eta_{\mathrm{CC}}$ are the absorption, exciton diffusion, charge transfer, and charge carrier collection efficiencies, respectively. Absorption efficiency, $\eta_{\mathrm{A}}$, is the fraction of photons absorbed, and it can simply be increased by using thicker

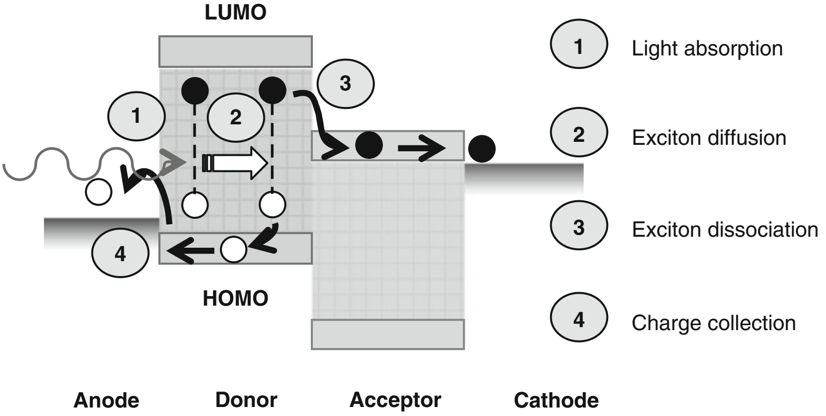

**Fig. 11** Schematic diagram of the basic working principle of an OPV device

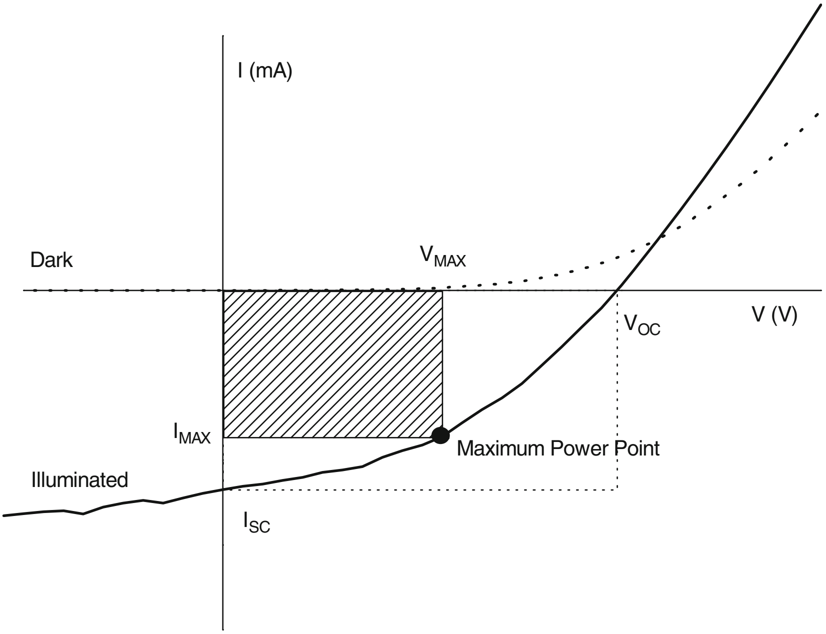

**Fig. 12** Typical current–voltage curves of an organic solar cell in the dark and under illumination. Important device parameters are also shown, including short-circuit current ($I_{SC}$), open-circuit voltage ($V_{OC}$), and the points of current and voltage ($I_{MAX}$ and $V_{MAX}$, respectively) that correspond to maximum power output

photoactive layers. However, exciton diffusion length invariably limits the thickness of the photoactive layer. Only photons absorbed within the exciton diffusion length from the donor–acceptor interface can survive the transport to the interface to subsequently dissociate into free charge carriers with a high yield, defined as the exciton diffusion efficiency, $\eta_{ED}$. The inherent trade-off between the $\eta_A$ and the $\eta_{ED}$ poses an upper limit of $\eta_{EQE}$. Fortunately, most organic materials possess high absorption coefficients of larger than $10^5$ cm$^{-1}$, providing the possibility for keeping the layer thickness as thin as possible (~exciton diffusion length) with highly absorptive properties.

## *3.2 Device Characteristics of an OPV Device*

In order to maximize the device performance, it is crucial to understand the parameters of an OPV device that form the rationale for the design of new organic materials or device architectures. A graph of current–voltage (*I*–*V*) characteristics is a common way to illustrate the photovoltaic response of an OPV device. Figure 12 depicts the typical *I*–*V* curves of an OPV device. In the dark, there is almost no current flowing through the devices. When the forward bias voltage becomes larger than the open-circuit voltage, current starts to flow. Under illumination, the current flows in a direction opposite to that of the injected currents, that is, *I*–*V* curve shifts downward. From the *I*–*V* curves, four device parameters can also be determined.

### 3.2.1 Short-Circuit Current

Short-circuit current ($I_{\mathrm{SC}}$) is the current under zero-applied bias voltage. It is the current that flows through an illuminated solar cell when there is no external resistance, that is, when the electrodes are simply connected or short circuited. $I_{\mathrm{SC}}$ is the maximum current that a device is able to produce, and it is strongly dependent on the absorption efficiency and exciton diffusion length in the photoactive materials. Particularly, it is linearly proportional to the $\eta_{\mathrm{EQE}}$ [54].

### 3.2.2 Open-Circuit Voltage

Open-circuit voltage ($V_{\mathrm{OC}}$) is the voltage at which the photogenerated current is balanced to zero (so-called flat band condition). It is the maximum possible voltage across an OPV device. $V_{\mathrm{OC}}$ is predominantly determined by the energy difference between the highest occupied molecular orbital (HOMO) of the donor and the lowest unoccupied molecular orbital (LUMO) of the acceptor [55, 56], that is, $qV_{\mathrm{OC}} = E_{\mathrm{HOMO}}$ (donor)–$SE_{\mathrm{LUMO}}$ (acceptor), where $q$ is the electronic charge, $E_{\mathrm{HOMO}}$ and $E_{\mathrm{LUMO}}$ are the energy levels of the photoactive materials, and $S$ is the slope of the linear fit.

### 3.2.3 Fill Factor

Fill factor (FF) is the ratio of the maximum power output of an OPV device to its theoretical power output if both current and voltage were at their maxima, $I_{\mathrm{SC}}$ and $V_{\mathrm{OC}}$, respectively [57]. It is used to characterize the shape of the *I*–*V* curves in the power-generating fourth quadrant.

$$\mathrm{FF} = P_{\mathrm{MAX}}/I_{\mathrm{SC}} \times V_{\mathrm{OC}} = I_{\mathrm{MAX}} \times V_{\mathrm{MAX}}/I_{\mathrm{SC}} \times V_{\mathrm{OC}}\,. \tag{3}$$

For a high FF, the shunt resistance should be very large to prevent leakage currents, and the series resistance should be very small to get a sharp rise in the forward current.

### 3.2.4 Power Conversion Efficiency

Power conversion efficiency (PCE) is the key quantity used to characterize the cell performance. It is a standard industry metric for solar cell performance, and it measures the ratio of the electrical power produced by the cell per unit area in watts, divided by the watts of incident light under certain specified conditions called "standard test conditions" [50]. In other words, it is the ratio of the amount of

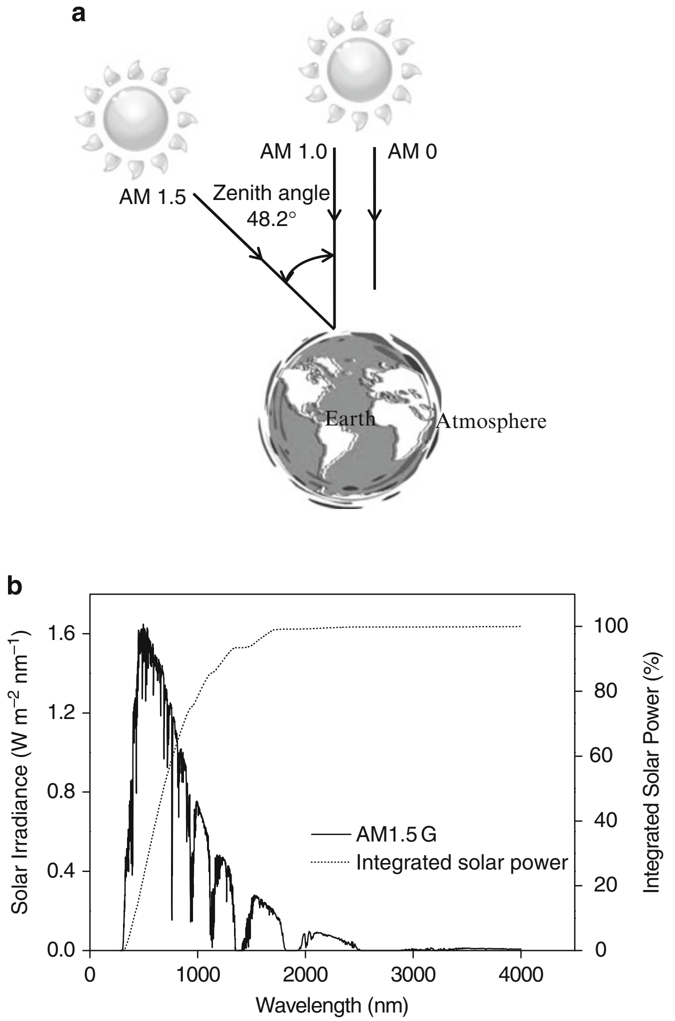

**Fig. 13** **(a)** Schematic diagram of different AM sunlight spectra. **(b)** Spectral irradiance (*solid line*) for AM1.5G sunlight and the integrated solar power

optical power produced by the OPV device relative to the power available in the incident solar radiation ($P_{\mathrm{IN}}$), given as

$$\mathrm{PCE} = P_{\mathrm{MAX}}/P_{\mathrm{IN}} = I_{\mathrm{SC}} \times V_{\mathrm{OC}} \times FF/P_{\mathrm{IN}}(\%). \tag{4}$$

Standard test conditions represent a set of conditions under which the solar cell can be evaluated and compared, including (1) irradiance intensity of 1,000 W $\mathrm{m}^{-2}$, (2) Air Mass (AM) 1.5 solar reference spectrum, and (3) the solar cell temperature during measurement of 25°C.

AM is a measure of how much sunlight traveled through the atmosphere to reach the earth's surface. This is usually denoted as "AM($x$)", where $x$ is the inverse of the cosine of the zenith angle of the sun [58]. A typical value for solar cell measurements is AM1.5, which means that the sun is at an angle of 48°. Figure 13a shows the schematic illustration of different AM sunlight spectra. Figure 13b depicts the spectral irradiance for AM1.5 global sunlight and the integrated solar power. The solar spectrum includes invisible ultraviolet (UV) light, the visible spectrum of colors, and the invisible infrared (IR) spectrum. Solar radiation includes wavelengths as short as 300 nm and as long as 4,045 nm. The amount of incoming photons across the UV, visible, and IR spectra is about 3%, 45%, and 52%, respectively. It is worth noting that harvesting as large a portion of the solar spectrum is important to increase $I_{SC}$, particularly for the red and near-infrared spectral regions. For example, absorbing light at $\lambda \leq 1.1$ μm (that is the optical bandgap of silicon) can collect up to 77% of the incident power. Using organic material with a low optical bandgap can effectively increase the $I_{SC}$.

### 3.2.5 Incident Photon to Current Efficiency

Incident photon to current efficiency (IPCE) is the efficiency of an OPV device as a function of the energy or wavelength of the incident radiation. Under monochromatic lighting at a particular wavelength, $\lambda$, it is defined as the number of photogenerated charge carriers contributing to the photocurrent per incident photon. It is simply the number of electrons measured under short-circuit current conditions, no applied bias, divided by the number of incident photons [58]. IPCE is defined as

$$\mathrm{IPCE} = 1.24 I_{SC}/(G \times \lambda)\,(\%), \tag{5}$$

where $G$ is the light density (in W cm$^{-2}$).

## 3.3 OPV Device Architecture

Nowadays, most of the OPV devices consist of two photoactive materials to form donor–acceptor heterojunction. Indeed, the photovoltaic effect in organic materials was first observed in single layers of organic materials, deposited between two metal electrodes of different work functions, to produce a rectifying device. These devices produced rather low PCE of only 0.01% [54]. Particularly, the reasons for the poor performance may be attributed to the low exciton dissociation rate. In single-layer devices, only the excitons that can remain intact long enough to reach the electrode can dissociate into free charge carriers. An estimation based on Onsager model for charge–pair dissociation revealed that exciton dissociation in the bulk of an organic material requires applied electric fields in excess of $10^6$ V cm$^{-1}$ to overcome the binding energy of an electron–hole pair and to have a considerable dissociation probability [59]. The breakthrough that led to an exponential growth of this OPV field was achieved by Tang in 1985 [60]. He introduced the concept of bilayer heterojunction, in which two organic layers with specific electron- or hole-transporting properties were sandwiched between the indium tin oxide (ITO)-coated glass as anode and a Ag cathode. Using a copper phthalocyanine (CuPc) as the donor and a perylene tetracarboxylic derivative as acceptor, a remarkably high PCE of 0.95% was recorded under simulated AM2 illumination with light intensity of 75 mW $\mathrm{cm}^{-2}$, an order of magnitude higher than that for single-layer OPV devices. Figure 14 illustrates a schematic diagram of a bilayer OPV device and the commonly used donor and acceptor materials, including CuPc [61–65], buckminsterfullerene ($C_{60}$) [61–69], 3,4,9,10-perylenetetracarboxylic bis-benzimidazole (PTCBI) [60, 64, 65], pentacene [68, 69], [6,6]-phenyl-$C_{61}$-butyric acid methyl ester (PCBM) [70–73], [6,6]-phenyl-$C_{71}$-butyric acid methyl ester ($PC_{70}BM$) [74, 75], and poly(3-hexylthiophene) (P3HT) [70, 72, 73]. The performance improvement is mainly attributed to the sharp increase in the exciton dissociation efficiency, in which the discontinuous HOMO and LUMO levels at the donor–acceptor interface can efficiently separate the bound electron–-hole pairs into free charge carriers. In addition, this bilayer device architecture can also enhance the spectral coverage within the solar spectrum due to the use of two photoactive materials. The use of separated charge transporting materials to form the donor–acceptor junction can further assist the transport of charge carriers to their respective electrodes, enhancing the charge collection efficiency. For bilayer OPV devices, efficient exciton dissociation at the donor–acceptor heterojunction takes place, provided the energy level offset for the HOMO or LUMO ($\Delta E_{\mathrm{HOMO}}$ or $\Delta E_{\mathrm{LUMO}}$, respectively) should be larger than the exciton binding energy ($E_{\mathrm{B}}$) in photoactive materials [76]. In particular, $\Delta E_{\mathrm{HOMO}}$ ($\Delta E_{\mathrm{LUMO}}$) should be larger than the acceptor (donor) exciton binding energy for efficient exciton dissociation in the acceptor (donor) [76]. $E_{\mathrm{B}}$ is the minimum energy needed to overcome the Coulomb electric force to separate the exciton into free electron and hole [76], and is given by the energy difference between the transport gap and optical gap of organic material, that is, $E_{\mathrm{B}} = E_{\mathrm{TRANS}} - E_{\mathrm{OPT}}$ [76, 77]. As shown in Fig. 15, transport gap is the energy difference between the HOMO and LUMO of the organic material while optical gap is determined from the low-energy absorption edge. For most organic materials, the $E_{\mathrm{B}}$ is within 0.2–2 eV [77].

Since then, many smart device configurations and high-performance materials have recently been developed to improve the photovoltaic responses. Encouraging progress with PCE up to 6.1% has been recently reported [74]. Here, we review various architectures that have been often exploited to optimize the device performance, including the introduction of exciton blocking layer (EBL), optical spacer, bulk heterojunction, low bandgap photoactive materials, and tandem structures.

### 3.3.1 Exciton Blocking Layer

As metal cathode is deposited onto the photoactive materials, the metal clusters may diffuse into the organic materials, creating a highly structured interface and

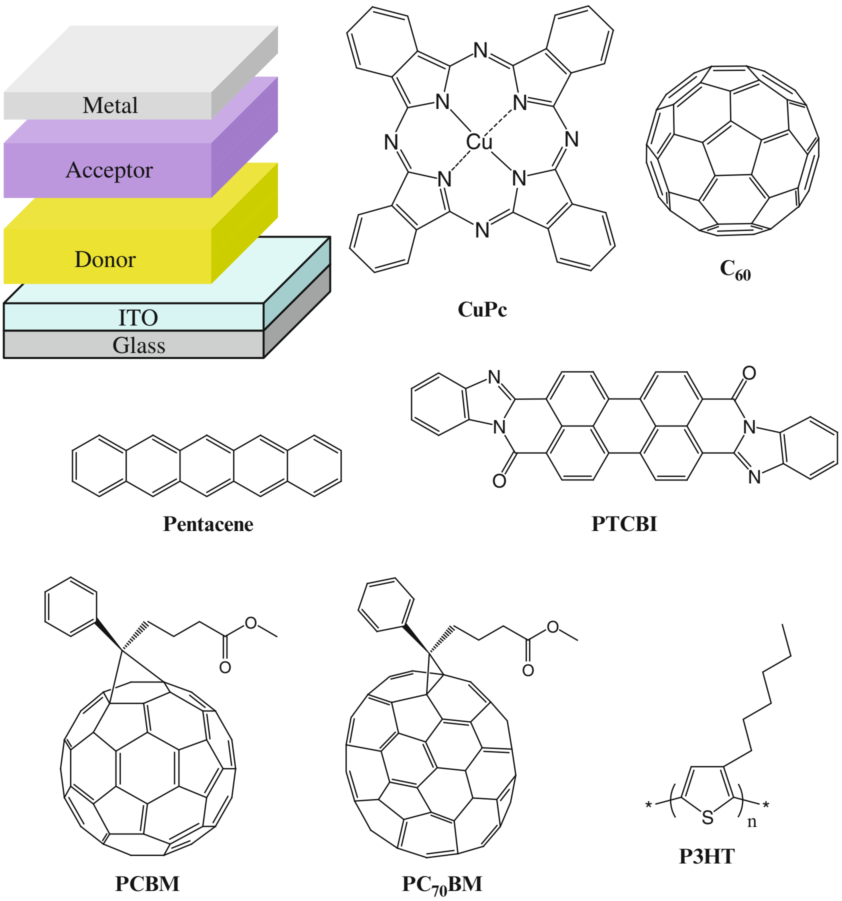

**Fig. 14** Typical device architecture of an organic solar cell and the commonly used small molecular and polymeric materials

rendering interface induced exciton recombination more likely. Particularly, defect states within the organic layer are induced which quench the excitons as well as trap charge carriers, leading to a high contact resistance at the acceptor–metal interface. This definitely limits the internal quantum efficiency of OPV devices. In order to solve this problem, Peumans and Forrest introduced bathocuproine (BCP) as an EBL inserted in between the acceptor layer and metal cathode [61]. With its large ionization potential ($I_P = 6.4$ eV) and large energy gap (3.5 eV), BCP acts as an effective EBL which blocks the diffusion of excitons to the cathode. This confinement of excitons significantly reduces the exciton quenching at the cathode, so that more excitons can contribute to the generation of electricity, and thus leads to efficiency enhancement. Particularly, for standard bilayer CuPc/$C_{60}$ OPV devices, a tenfold increase in PCE (~1.5%) can be achieved for devices with BCP as EBL, as compared to that without EBL layer (~0.017%) [63].

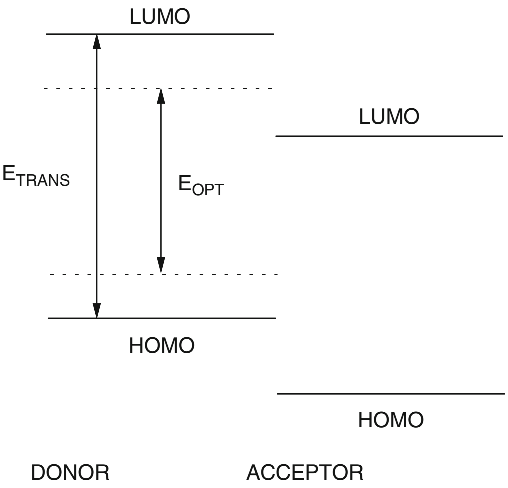

**Fig. 15** Schematic energy level diagram of a donor–acceptor interface

However, the organic material employed must fulfill the basic requirements for an efficient EBL. The film needs to have a high electron affinity and a high $I_P$, such that it allows efficient electron injection while blocking exciton diffusion [52, 61]. Furthermore, it needs to have a low optical absorption coefficient and a high electrical conductivity, such that a good device performance can be achieved even when a large variety of optimum optical thicknesses are required for different OPV devices. This definitely limits the choice of materials that can be employed. More importantly, efficient electron transport in the EBL occurs mainly through defect states induced during the metal cathode deposition. If the EBL is too thick, the charge collection efficiency will be reduced as the cell resistance increases. Particularly, the thickness of EBL is around 5–10 nm, depending on the depth of metal atoms penetrating into the organic material.

### 3.3.2 Optical Spacer

Due to the high reflectivity of metal cathode, optical interference between the incident (from the transparent anode side) and back-reflected light occurs, in which the intensity of the light is almost zero at the metallic cathode [70]. This leads to a relatively large fraction of the photoactive layer positioned in a dead-zone, significantly reducing the photogeneration of charge carriers. In order to overcome this problem, a concept of optical spacer that spatially redistributes the light intensity inside the device is introduced. An optical spacer is a highly transparent layer inserted in between the acceptor layer and the cathode. It is used for modulating the intensity of the incident light, such that intensity maximum would be close to the donor–acceptor interface where absorption and charge dissociation are efficient, as shown in Fig. 16. Depending on the optical properties

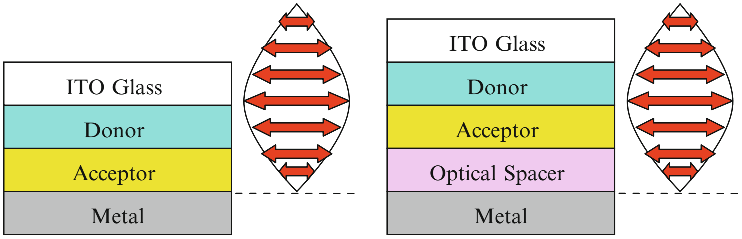

**Fig. 16** Schematic diagram of the spatial distribution of the optical electric field strength inside the devices with a structure of ITO/active layer/metal and ITO/optical spacer/active layer/metal

(optical absorption spectra and refractive index) of the active organic materials used in the OPV devices, different thicknesses of an optical spacer (typically 10–30 nm) should be used to achieve the optimum optical design [70, 78–80]. Basically, the films as optical spacer must be a good electron-transporting material and is highly transparent within the solar spectrum. Furthermore, it needs to have an excellent energy level matching with the LUMO of the acceptor layer as well as the Fermi level of the metal cathode for electron injection [70, 78–80].

Recently, Kim et al. [70] demonstrated the effectiveness of this concept by using a solution-based sol–gel process to prepare a titanium oxide ($TiO_x$) as an optical spacer inserted in between the polymeric matrix and the Al cathode. It is well known that $TiO_x$ is a good electron acceptor and electron-transporting material, as confirmed by its use in dye-sensitized solar cells. As expected, this amorphous $TiO_x$ layer exhibited a high electron mobility of $1.7 \times 10^{-4}$ $cm^2$ $V^{-1}$ $s^{-1}$, and a relatively large optical bandgap of 3.7 eV. More importantly, $TiO_x$ had a good energy level matching with the LUMO of polymeric P3HT:PCBM matrix as well as the metal cathode, satisfying the electronic structure requirements of an optical spacer. By employing $TiO_x$ as optical spacer, the polymeric OPV devices demonstrated substantially improved photovoltaic responses. Under AM1.5 illumination with light intensity of 90 mA $cm^{-2}$, such device exhibited a high $I_{SC}$ of 11.1 mA $cm^{-2}$, a $V_{OC}$ of 0.61 V, a FF of 0.66, and a PCE of 5.0%. These values were significantly better than those ($I_{SC} = 7.5$ mA $cm^{-2}$, $V_{OC} = 0.51$ V, FF = 0.54, and PCE of 2.3%) of devices without an optical spacer. The performance improvement could be rationalized in terms of the increased absorption in the photoactive layer that arises from a better match of the spatial distribution of the light intensity to the maximum position of the polymeric P3HT:PCBM film.

### 3.3.3 Bulk Heterojunction

As mentioned in Sect. 3.3, due to the short exciton diffusion length in most organic materials (typically 3–40 nm), only photons absorbed within the exciton diffusion length from the donor–acceptor interface can survive the transport to the interface to subsequently dissociate into free charge carrier with a high yield. This invariably limits the thickness of the photoactive layer and thus the absorption efficiency. In addition, Yang and Forrest [53] recently reported that the $\eta_{\mathrm{EQE}}$ of devices with planar bilayer structure shows a strong dependence on exciton diffusion length. At larger photoactive layer thicknesses, absorption shifts toward the ITO–donor interface, where the narrow exciton distribution results in decreased $\eta_{\mathrm{ED}}$ and hence $\eta_{\mathrm{EQE}}$. For standard CuPc/$C_{60}$ bilayer device, the $\eta_{\mathrm{ED}}$ dropped from 0.6 in CuPc (10 nm)/$C_{60}$ (20 nm) to 0.2 in CuPc (20 nm)/$C_{60}$ (40 nm), and approached to 0 for total photoactive layer thickness increases to 100 nm.

The concept of bulk heterojunction circumvents the exciton diffusion limitation in the bilayer device structures. In 1995, Yu et al. [81] first utilize this approach by simply dispersing fullerene in a conjugated polymer and then spin coating the solution onto the device. Devices with the composite polymer film ($C_{60}$: MEH-PPV, where MEH-PPV is poly(2-methoxy-5-(2′-ethyl-hexyloxy)-1,4-phenylene vinylene)) showed a dramatically increased PCE of 2.9%, two orders of magnitude higher than that without the $C_{60}$ dispersion. Bulk heterojunction consists of an intimate mixture of donor and acceptor materials via blending polymers or coevaporation methods. The mixed layer creates a spatially distributed donor–acceptor interface, where all excitons generated can be efficiently dissociated into free charge carriers throughout the bulk heterojunction, giving ~100% $\eta_{\mathrm{ED}}$. Figure 17 depicts the schematic diagrams of the photovoltaic processes for both bilayer and bulk heterojunction devices. In addition, the bulk heterojunction essentially extends the photoactive layer thickness and decreases the charge carrier recombination probability, leading to a higher dark current and $I_{\mathrm{SC}}$. Extensive studies had been carried out to investigate the charge carrier transport and photogeneration mechanisms within bulk heterojunction. Ultrafast spectroscopic analysis revealed that ultrafast charge transfer (~45 fs) from the conjugated polymers to fullerenes has been observed, resulting in a nearly unity charge transfer efficiency [82]. Yang and Forrest recently further supported that the exciton diffusion efficiency is equal to one for all photoactive layer thicknesses due to the highly distributed donor–acceptor interface [53]. This definitely provides a simple means to extend the photoactive layer thickness and thus increasing the absorption efficiency.

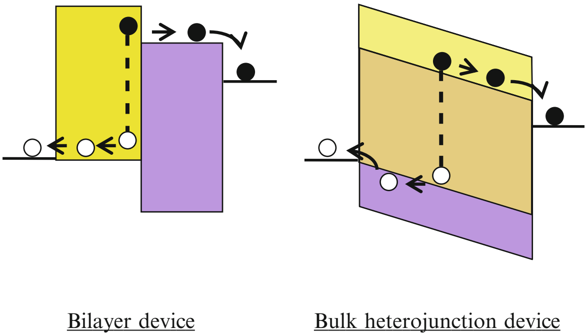

**Fig. 17** Schematic diagram of photovoltaic processes for bilayer and bulk heterojunction devices

However, the morphology, or microstructure, of the mixed layer of bulk heterojunction plays a crucial role in determining the device efficiency. In 2001, Shaheen et al. [83] demonstrated that the photovoltaic responses of polymeric OPV devices were controlled by the morphology of the polymer layer. It was found that the conformation of polymer chains was controlled by the selection of the casting solvents, in which aromatic solvents (e.g., dichlorobenzene or chlorobenzene) could prevent the formation of isolated regions of polymer and PCBM in the film and enhance the polymer chain packing to increase hole mobility. Particularly, devices with chlorobenzene-casted film had a high $I_{SC}$ of 5.25 mA cm$^{-2}$, a $V_{OC}$ of 0.82 V, and a FF of 0.61, corresponding to a PCE of 2.5%. These values were comparatively higher than those of devices with toluene-casted film ($I_{SC} = 2.33$ mA cm$^{-2}$, $V_{OC} = 0.82$ V, FF = 0.50, and PCE = 0.9%). Furthermore, the intrinsically low carrier mobilities in the bulk heterojunction are the bottleneck for maximizing the $\eta_{EQE}$ of OPV devices. Rand et al. [84] found that in the CuPc:$C_{60}$ mixture (1:1 by weight), the electron and hole mobilities were reduced by more than one order of magnitude compared to that of the neat CuPc or $C_{60}$ films. In particular, hole mobility of the mixed film at zero electric field is $3.3 \times 10^{-6}$ cm$^2$ V$^{-1}$ s$^{-1}$, two orders of magnitude lower than that of the pristine CuPc film ($7.4 \times 10^{-4}$ cm$^2$ V$^{-1}$ s$^{-1}$). This led to a significantly lower charge carrier collection efficiency ($\eta_{CC}$ ~ 0.4), resulting from a large recombination rate at the increased interface area, as compared to that with planar device structure ($\eta_{CC}$ = 1.0) [53].

### 3.3.4 Low Bandgap Photoactive Materials

One of the major obstacles for achieving high PCE is the limited spectral overlap between the absorption of photoactive materials and the solar spectrum, resulting in a low photocurrent. Indeed, ~62% of the total solar photon flux is at wavelengths $\lambda > 600$ nm with approximately 40% in the red and near-infrared (NIR) spectrum at $600 < \lambda < 1{,}000$ nm. However, the optical bandgap of most organic photoactive materials is not optimized with respect to the solar spectrum, in which only 20–30% of solar spectrum can be absorbed. For instance, CuPc, a commonly used donor material in OPV devices, has an absorption spectrum that falls off at $\lambda > 700$ nm [80, 84]. This suggests that new materials need to be developed that can absorb NIR radiation, and effectively convert the absorbed photons into electricity.

Various new organic materials with low optical bandgap and broad spectral coverage extending into the NIR radiation have been designed and synthesized. With the extensive device engineering efforts, encouraging power conversion efficiencies of 4–5% have been demonstrated for the NIR OPV devices [71, 73, 74, 85, 86]. Here, there are several examples of novel low optical bandgap organic materials that are promising candidates for further exploration in OPV devices with real applications. In 2006, Mühlbacker et al. [85] had designed and synthesized a new polymeric material, poly[2,6-(4,4-bis-(2-ethylhexyl)-4*H*-cyclopenta[2,1-*b*;3,4-*b*′]-dithiophene)-*alt*-4,7-(2,1,3-benzothiadiazole)] (PCPDTBT). PCPDTBT

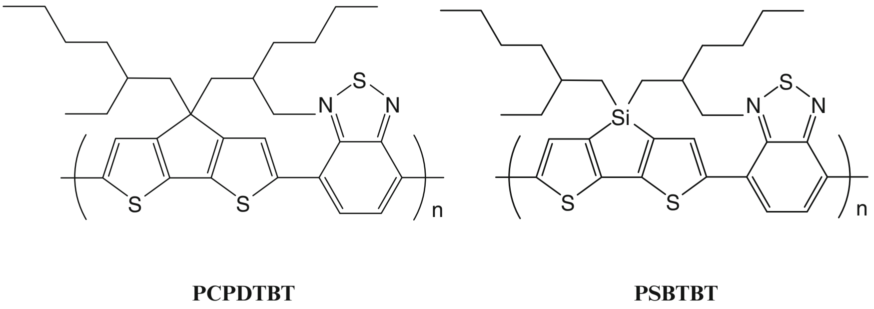

**Fig. 18** Chemical structures of PCPDTBT and PSBTBT

was the first candidate of a new class of copolymers utilizing a cyclopentadithiophene unit as the donor block in the polymer chain, and it exhibited a low optical bandgap of 1.46 eV with spectral coverage extending up to 900 nm. In addition, the PCPDTBT/$P_{70}$BM-based polymeric OPV devices attained a high PCE of 3.2%. Later, Hou et al. [86] modified the PCPDTBT by substituting the 9-position of the fluorene units with silicon atoms in order to improve the hole-transporting property of the material and two 2-ethylhexyl side chains attached to the silicon atom to enhance the solubility to synthesize a novel silole-containing polymer, poly[(4,4′-bis(2-ethylhexyl)dithieno[3,2-*b*;2′,3′-*d*]silole)-2,6-diyl-*alt*-2,1,3-benzothiadiazole-4,7-diyl] (PSBTBT). Figure 18 shows the chemical structures of PCPDTBT and PSBTBT. This polymer performed a high hole mobility of $3 \times 10^{-3}$ $cm^2$ $V^{-1}$ $s^{-1}$, that was three times higher than that for the unmodified polymer. In addition, such polymeric OPV device exhibited a high PCE of 5.1% under AM1.5G (G: Global) illumination with light intensity of 100 mW $cm^{-2}$.

Very recently, Heeger's group reported a polymeric OPV device with the world record PCE of 6.1% under 1 sun AM 1.5G irradiation [74]. This success relied on the use of alternating copolymer based on poly(2,7-carbazole) derivatives, with a suitable electron-deficient moieties to tune the electronic energy gap and absorption spectrum into the NIR region. In particular, the smaller bandgap of polymer can harvest a larger fraction of the solar radiation spectrum, while the deeper HOMO energy of the carbazole group can effectively increase the $V_{OC}$ of the devices. Such polymeric OPV device attained a high $I_{SC}$ of 10.6 mA $cm^{-2}$, high $V_{OC}$ of 0.88 V, and FF of 0.66, resulting in an impressive PCE of 6.1%. More importantly, from the IPCE measurement, it was found that the internal quantum efficiency is close of 100%, implying that essentially every absorbed photon resulted in a separated pair of charge carriers and that all photogenerated carriers could be collected at the respective electrodes.

### 3.3.5 Tandem Structures

Since the first demonstration of tandem device structure by Kido et al. [87], this concept has been widely used in OLEDs for improving the device performance

[33–35]. Tandem structure consists of two or more individual subcells connected electrically in series via charge connecting unit. Under operation, charge carriers will be generated within the connecting unit and are injected into the adjoining electroluminescence (EL) elements. In principle, both luminous efficiency and operation lifetime can be proportionally increased with the number of EL units. This approach can also be employed to achieve white light by the combination of the two or more complementary colors.

This concept of tandem OPV structure had also been realized by Xue et al. [66], in which two individual OPV cells were connected in series by an ultrathin (~5 Å) discontinuous metallic film as an interlayer. The metal nanoclusters acted as efficient charge recombination centers that allowed these subcells to operate without incurring a voltage drop at the junction between two subcells. To obtain the series configuration, an inverse oriented heterojunction between the acceptor layer of one cell and the donor layer of the adjacent cell was employed. Such tandem OPV devices exhibited a high $V_{\mathrm{OC}}$, close to the sum of the $V_{\mathrm{OC}}$ of two subcells, and high PCE of 5.7%. Kim et al. [88] also demonstrated a tandem polymeric OPV device by stacking two subcells (PCPDTBT:PCBM and P3HT:$\mathrm{PC}_{70}$BM) together via a thin $\mathrm{TiO}_x$ interlayer. This resulted in an impressive PCE of 6.5%.

However, due to the optical interference effects and the thickness-dependent optical properties of the thin interlayer, realization of tandem structure needs careful optimization of the respective photoactive layer thickness of each subcell. In particular, the cell structure should be arranged for making the front cell rich in the longer wavelength absorbing materials and the back cell rich in the shorter wavelength materials [66, 88]. In addition, the current of the tandem OPV devices is determined by the current generation in the lowest subcell [88]. This significantly poses an upper limit on the PCE of tandem devices.

## 3.4 Challenges of OPV Devices

With the continuous efforts on the development of new organic materials and innovative device engineering, the PCE of OPV devices has been steadily improved up to 6.1%; however, this efficiency is still not sufficient to meet the realistic specifications for commercialization. The major obstacle for achieving high PCE is the mismatch of the absorption of photoactive materials to the terrestrial solar spectrum. In particular, the optical bandgap of most photoactive organic materials is much larger than the maximum photon flux at 1.8 eV, wasting over 60% of the solar spectrum. Scharber et al. [55] had systematically studied the dependence of $V_{\mathrm{OC}}$ on the bandgap and HOMO levels of 26 conjugated polymers and predicted the limited efficiency of bulk heterojunction OPV devices. It was found that PCE of 10% can theoretically be achieved for the PCBM-based polymeric OPV device, provided that the donor polymer must have a bandgap $<1.74$ eV and a LUMO level $<-3.92$ eV, assuming that the FF and the average $\eta_{\mathrm{EQE}}$ remain equal to 0.65. Meanwhile, Rand et al. [56] presented a comprehensive device model to predict the photovoltaic responses of small molecular-based OPV devices. This model infers that the maximum PCE as high as 12% is feasible for an optimized double heterostructure OPV device. However, its success relies on the development of new organic materials, in which the donor and acceptor materials should have optical bandgap of 1.5 and 1.8 eV, respectively, and a large interface offset energy, that is, $\Delta = I_P$ (donor) − $E_A$ (acceptor) = 1.1 eV. This suggests that new photoactive materials with low optical bandgap are definitely needed to be developed.

## 4 Conclusions

With the growing demand on energy consumption, there is an urgent need for implementing more energy saving measures. Many nations have committed on their new policies to implement the ways for saving energy and promoting it. Particularly, solid-state organic devices, especially WOLEDs and organic solar cells, are targeted as effective ways for reducing the energy consumption and developing renewable energy in the world. Because of high $\eta_P$ and ultra-low costs of organic materials, WOLEDs and organic solar cells are gaining acceptance as the new generation of solid-state lighting sources to replace and complement the incandescent bulbs and an alternative type of solar cells to dislodge or complement the traditional Si solar cell for electricity generation, respectively. Indeed, WOLEDs with fluorescent tube efficiency as high as 102 lm $W^{-1}$ and organic solar cells with high PCE of 6.1% have been achieved in the laboratory. With the continuous efforts on improving their lifetimes and reducing the manufacturing cost, WOLEDs and organic solar cells have a very bright future to be used widely.

**Acknowledgments** This work has been supported by the University Grants Committee Areas of Excellence Scheme (AoE/P-03/08) and the Strategic Research Theme on Molecular Materials of The University of Hong Kong.

## References

1. US Energy Information Administration, International Energy Outlook 2009 (August 2009)
2. US Energy Information Administration, Annual Energy Outlook 2009 (March 2009)
3. D'Andrade BW, Forrest SR (2004) White organic light-emitting devices for solid-state lighting. Adv Mater 16:1585–1595
4. US Energy Information Administration, Annual Energy Review 2006 (June 2007)
5. US Department of Energy (2002) National lighting inventory and energy consumption estimate, vol 1. Navigant Consulting, Washington DC
6. Reinkek S, Lindner F, Schwartz G, Seidler N, Walzer K, Lüssem B, Leo K (2009) White organic light-emitting diodes with fluorescent tube efficiency. Nature 459:234–238
7. Su SJ, Gonmori E, Sasabe H et al (2008) Highly efficient organic blue- and white-light-emitting devices having a carrier- and exciton-confining structure for reduced efficiency roll-off. Adv Mater 20:4189–4194

8. Schwartz G, Reineke S, Walzer K et al (2008) Reducing efficiency roll-off in high-efficiency hybrid white organic light-emitting diodes. Appl Phys Lett 92:053311
9. Forrest SR, Bradley DDC, Thompson ME (2003) Measuring the efficiency of organic light-emitting devices. Adv Mater 15:1043–1048
10. Commission Internationale de L'éclairage (CIE) (1986) Colorimetry, Publication Report No. 15.2
11. Borbély Á, Sámson Á, Schanda J (2001) The concept of correlated color temperature revisited. Color Res Appl 26:450–457
12. Commission Internationale de L'éclairage (CIE) (1974) Method of measuring and specifying color rendering properties of light sources, Publication Report No. 13.2
13. Joint ISO/CIE Standard: CIE standard illuminants for colorimetry provide explanations and descriptions of the CIE standard illuminants. ISO 10526:1999/CIE S005/E-1998
14. D'Andrade BW, Holmes RJ, Forrest SR (2004) Efficient organic electrophosphorescent white-light-emitting device with a triple doped emissive layer. Adv Mater 16:624–628
15. Lee MT, Lin JS, Chu MT et al (2008) Improvement in carrier transport and recombination of white phosphorescent organic light-emitting devices using a composite blue emitter. Appl Phys Lett 93:133306
16. Eom SH, Zheng Y, Wrzesniewski E et al (2009) White phosphorescent organic light-emitting devices with dual triple-doped emissive layers. Appl Phys Lett 94:153303
17. Wang Q, Ding J, Ma D et al (2009) Harvesting excitons via two parallel channels for efficient white organic LEDs with nearly 100% internal quantum efficiency: fabrication and emission-mechanism analysis. Adv Funct Mater 19:84–95
18. Wang Q, Ding J, Ma D et al (2009) Highly efficient single-emitting-layer white organic light-emitting diodes with reduced efficiency roll-off. Appl Phys Lett 94:103503
19. Sun Y, Giebink NC, Kanno H et al (2006) Management of singlet and triplet excitons for efficient white organic light-emitting devices. Nature 440:908–912
20. Schwartz G, Fehse K, Pfeiffer M et al (2006) Highly efficient white organic light emitting diodes comprising an interlayer to separate fluorescent and phosphorescent regions. Appl Phys Lett 89:083509
21. Sun Y, Forrest SR (2007) High-efficiency white organic light emitting devices with three separate phosphorescent emission layers. Appl Phys Lett 91:263503
22. Schwartz G, Pfeiffer M, Reineke S et al (2007) Harvesting triplet excitons for fluorescent blue emitters in white organic light-emitting diodes. Adv Mater 19:3672–3676
23. Chang CH, Lin YH, Chen CC et al (2009) Efficient phosphorescent white organic light-emitting devices incorporating blue iridium complex and multifunctional orange-red osmium complex. Org Electron 10:1235–1240
24. Luo J, Li X, Hou Q et al (2007) High-efficiency white-light emission from a single copolymer: fluorescence blue, green, and red chromophores on a conjugated polymer backbone. Adv Mater 19:1113–1117
25. Liu J, Shao SY, Chen L et al (2007) White electroluminescence from a single polymer system: improved performance by means of enhanced efficiency and red-shifted luminescence of the blue-light-emitting species. Adv Mater 19:1859–1863
26. Thompson J, Blyth RIR, Mazzeo M et al (2001) White light emission from blends of blue-emitting organic molecules: a general route to the white organic light-emitting diode? Appl Phys Lett 79:560–562
27. D'Andrade BW, Brooks J, Adamovich V et al (2002) White light emission using triplet excimers in electrophosphorescent organic light-emitting devices. Adv Mater 14:1032–1036
28. Williams EL, Haavisto K, Li J et al (2007) Excimer-based white phosphorescent organic light emitting diodes with nearly 100% internal quantum efficiency. Adv Mater 19:197–202
29. Mazzeo M, Pisignano D, Della Sala F et al (2003) Organic single-layer white light-emitting diodes by exciplex emission from spin-coated blends of blue-emitting molecules. Appl Phys Lett 82:334–336

30. Palilis C, Mäkinen AJ, Uchida M et al (2003) Highly efficient molecular organic light-emitting diodes based on exciplex emission. Appl Phys Lett 82:2209–2211
31. Tong QX, Lai SL, Chan MY et al (2007) High-efficiency nondoped white organic light-emitting devices. Appl Phys Lett 91:023503
32. Kido J, Nakada T, Endo J et al (2002) High efficiency organic EL devices having charge generation layer. In: Neyts K, De Visschere P, Poelman D (eds) Proceedings of the 11th international workshop on inorganic and organic electroluminescence and 2002 international conference on the science and technology of emissive displays and lighting, Universiteit Ghent, Ghent, Belgium 2002, p 539
33. Liao LS, Klubek KP, Tang CW (2004) High-efficiency tandem organic light-emitting diodes. Appl Phys Lett 84:167–169
34. Tsutsui T, Terai M (2004) Electric field-assisted bipolar charge spouting in organic thin-film diodes. Appl Phys Lett 84:440–442
35. Lai SL, Chan MY, Fung MK et al (2007) Copper hexadecafluorophthalocyanine and copper phthalocyanine as a pure organic connecting unit in blue tandem organic light-emitting devices. J Appl Phys 101:014509
36. Chan MY, Lai SL, Lau KM et al (2007) Influences of connecting unit architecture on the performance of tandem organic light-emitting devices. Adv Funct Mater 17:2509–2514
37. Krummacher BC, Choong V-E, Mathai MK et al (2006) Highly efficient white organic light-emitting diode. Appl Phys Lett 88:113506
38. Ji W, Zhang L, Gao R et al (2008) Top-emitting white organic light-emitting devices with down-conversion phosphors: theory and experiment. Opt Express 16:15489–15494
39. NanoMarkets LC, OLED Lighting Markets 2008 (September 2008)
40. US Department of Energy, Solid-State Lighting Research and Development Portfolio: Technology Research and Development Plan FY'07-FY'12., Navigant Consulting, Inc. and Radcliffe Advisors (January 2007)
41. Optrex Europe GmbH homepage (http://www.optrex.de)
42. OSRAM homepage (http://www.osram-os.com/appsos/showroom/)
43. Global Research Blog website (http://ge.geglobalresearch.com/blog/worlds-first-demonstration-of-roll-to-roll-processed-oleds/)
44. eMercedesBenz website (http://www.emercedesbenz.com)
45. Yano Research Institute Ltd, World Solar Cell Market: Key Research Findings 2009 (http://www.yanoresearch.com). Figures are reproduced with permission from Yano Research Institute
46. LG Electronics website (http://www.lge.com)
47. Eindhoven University of Technology (2008, May 14). New world record for important class of solar cells
48. National Renewable Energy Laboratory (NREL) Newsroom, NREL of the US Department of Energy (http://www.nrel.gov/news/)
49. University of Delaware (2007, July 23). UD-led team sets solar cell record, joins Dupont on $100 million project
50. Wadell AL, Forrest SR (2006) High power organic solar cells from efficient utilization of near-infrared solar energy. Mater Eng News pp 10–11
51. Hoppe H, Sariciftci NS (2004) Organic solar cells: an overview. J Mater Res 19:1924–1945
52. Peumans P, Yakimov A, Forrest SR (2003) Small molecular weight organic thin-film photodetectors and solar cells. J Appl Phys 93:3693–3723
53. Yang F, Forrest SR (2008) Photocurrent generation in nanostructured organic solar cells. ACS Nano 2:1022–1032
54. Rand BP, Genoe J, Heremans P et al (2007) Solar cells utilizing small molecular weight organic semiconductors. Prog Photovolt Res Appl 15:659–676
55. Scharber MC, Mühlbacher D, Koppe M et al (2006) Design rules for donors in bulk-heterojunction solar cells – towards 10% energy-conversion efficiency. Adv Mater 18:789–794

56. Rand BP, Burk DP, Forrest SR (2007) Offset energies at organic semiconductor heterojunctions and their influence on the open-circuit voltage of thin-film solar cells. Phys Rev 75:115327
57. Nunzi JM (2002) Organic photovoltaic materials and devices. C R Phys 3:523–542
58. Rostalski J, Meissner D (2000) Monochromatic versus solar efficiencies of organic solar cells. Sol Energy Mater Sol Cells 61:87–95
59. Onsager L (1938) Initial recombination of ions. Phys Rev 54:554–557
60. Tang CW (1986) Two-layer organic photovoltaic cell. Appl Phys Lett 48:183–185
61. Peumans P, Forrest SR (2001) Very-high-efficiency double-heterostructure copper phthalocyanine/$C_{60}$ photovoltaic cells. Appl Phys Lett 79:126–128
62. Uchida S, Xue J, Rand BP et al (2004) Organic small molecular solar cells with a homogeneously mixed copper phthalocyanine: $C_{60}$ active layer. Appl Phys Lett 84:4218–4220
63. Vogel M, Doka S, Breyer Ch, Lux-Steiner MCh, Fostiropoulos K (2006) On the function of a bathocuproine buffer layer in organic photovoltaic cells. Appl Phys Lett 89:163501
64. Peumans P, Uchida S, Forrest SR (2003) Efficient bulk heterojunction photovoltaic cells using small-molecular-weight organic thin films. Nature 425:158–162
65. Xue J, Uchida S, Rand BP et al (2004) Asymmetric tandem organic photovoltaic cells with hybrid planar-mixed molecular heterojunctions. Appl Phys Lett 85:5757–5759
66. Shao Y, Sista S, Chu CW et al (2007) Enhancement of tetracene photovoltaic devices with heat treatment. Appl Phys Lett 90:103501
67. Mayer AC, Lloyd MT, Herman DJ (2004) Postfabrication annealing of pentacene-based photovoltaic cells. Appl Phys Lett 85:6272–6274
68. Yoo S, Domercq B, Kippelen B (2004) Efficient thin-film organic solar cells based on pentacene/$C_{60}$ heterojunctions. Appl Phys Lett 85:5427–5429
69. Potscavage WJ, Yoo S, Domercq B et al (2007) Encapsulation of pentancene/$C_{60}$ organic cells with $Al_2O_3$ deposited by atomic layer deposition. Appl Phys Lett 90:253511
70. Kim JY, Kim SH, Lee HH et al (2006) New architecture for high-efficiency polymer photovoltaic cells using solution-based titanium oxide as an optical spacer. Adv Mater 18: 572–576
71. Liang Y, Wu Y, Feng D et al (2009) Development of new semiconducting polymers for high performance solar cells. J Am Chem Soc 131:56–57
72. Padinger F, Rittberger RS, Sariciftci NS (2003) Effects of postproduction treatment on plastic solar cells. Adv Funct Mater 13:85–88
73. Li G, Shrotriya V, Huang J et al (2005) High-efficiency solution processable polymer photovoltaic cells by self-organization of polymer blends. Nat Mater 4:864–868
74. Park SH, Roy A, Beaupré S et al (2009) Bulk heterojunction solar cells with internal quantum efficiency approaching 100%. Nat Photonics. doi:10.1038/NPHOTON.2009.69
75. Peet J, Kim JY, Coates NE et al (2007) Efficiency enhancement in low-bandgap polymer solar cells by processing with alkane dithiols. Nat Mater 6:497–500
76. Peumans P, Forrest SR (2004) Separation of geminate charge-pairs at donor-acceptor interfaces in disordered solid. Chem Phys Lett 398:27–31
77. Djurovich PI, Mayo EI, Forrest SR et al (2009) Measurement of the lowest unoccupied molecular orbital energies of molecular organic semiconductors. Org Electron 10:515–520
78. Hänsel H, Zettl H, Krausch G et al (2003) Optical and electrical contributions in double-heterojunction organic thin-film solar cells. Adv Mater 15:2056–2060
79. Stübinger T, Brütting W (2001) Exciton diffusion and optical interference in organic donor-acceptor photovoltaic cells. J Appl Phys 90:3632–3641
80. Chan MY, Lai SL, Lau KM et al (2006) Application of metal-doped organic layer both as exciton blocker and optical spacer for organic photovoltaic devices. Appl Phys Lett 89:163515
81. Yu G, Gao J, Hummelen JC et al (1995) Polymer photovoltaic cells – enhanced efficiencies via a network of internal donor-acceptor heterojunctions. Science 270:1789–1791

82. Brabec CJ, Zerza G, Cerullo G et al (2001) Tracing photoinduced electron transfer process in conjugated polymer/fullerene bulk heterojunctions in real time. Chem Phys Lett 340:232–236
83. Shaheen SE, Brabec CJ, Sariciftci NS et al (2001) 2.5% efficient organic plastic solar cells. Appl Phys Lett 78:841–843
84. Rand BP, Xue J, Uchida S et al (2005) Mixed donor-acceptor molecular heterojunctions for photovoltaic applications. I. Materials properties. J Appl Phys 98:124902
85. Mühlbacher D, Scharber M, Morana M et al (2006) High photovoltaic performance of a low-bandgap polymer. Adv Mater 18:2884–2889
86. Hou J, Chen HY, Zhang S et al (2008) Synthesis, characterization, and photovoltaic properties of a low bandgap polymer based on silole-containing polythiophenes and 2, 1, 3-benzothiadiazole. J Am Chem Soc 130:16144–16145
87. Kido J, Nakada T, Endo J et al (2002) High efficiency organic EL devices having charge generation layer. In: Neyts K, De Visschere P, Poelman D (eds) Proceedings of the 11th international workshop on inorganic and organic electroluminescence and 2002 international conference on the science and technology of emissive displays and lighting, Universiteit Ghent, Ghent, Belgium, p 539
88. Kim JY, Lee K, Coates NE et al (2007) Efficient tandem polymer solar cells fabricated by all-solution processing. Science 317:222–225